WORLD METEOROLOGICAL ORGANIZATION | GLOBAL ATMOSPHERE WATCH

No. 9 – JULY 2025

WMO AIRBORNE DUST BULLETIN

Overview of global airborne dust in 2024

The global annual mean surface dust concentration in 2024 (12.5 μg m^{-3}, see Figure 1(a)) was slightly lower than that in 2023 (12.7 μg m^{-3}, see *WMO Airborne Dust Bulletin, No. 8*). This decrease in 2024 is mainly attributed to reduced dust emissions from several dust-active regions around the world, such as central-eastern North Africa, the north-western Arabian Peninsula, the Thar Desert, northern India, western Central Asia, the Taklamakan Desert and the Gobi Desert. However, annual mean surface dust concentrations over western North Africa, the Atlantic Ocean, the south-eastern Arabian Peninsula and central Australia in 2024 were higher than those in 2023.

Spatially, the estimated peak annual mean surface dust concentration (~800–1 100 μg m^{-3}) in 2024 was located in some areas of Chad in north-central Africa, which is also the location of the Bodélé Depression, a known key emission source. In the southern hemisphere, dust concentrations reached their highest level (~150–300 μg m^{-3}) in parts of central Australia and the west coast of South Africa. Wind-driven dust aerosols may be transported from these typical dust source areas to many regions of the world, over distances of hundreds to thousands of kilometres. The regions that are most vulnerable to long-range transport of dust are: the northern tropical Atlantic Ocean between West Africa and the Caribbean; South America; the Mediterranean Sea; the Arabian Sea; the Bay of Bengal; and central-eastern China. In 2024, the transatlantic transport of African dust invaded various locations throughout the Americas, including parts of the Caribbean Sea region.

In the most affected areas, the surface dust concentration in 2024 was higher than the climatological mean (1981–2010). Exceptions to this were: most of west-central Africa, encompassing major portions of Algeria, Mali, Mauritania, Senegal, Niger, Chad, Sudan, Nigeria and Libya; the Arabian Peninsula and Iraq; western Central Asia; Pakistan; southern Mongolia and north-central China; and central Australia (Figure 1(b)). Hotspots with significantly higher dust concentrations were identified in: South America, encompassing the Bolivarian Republic of Venezuela, Colombia and north-western Brazil; southern

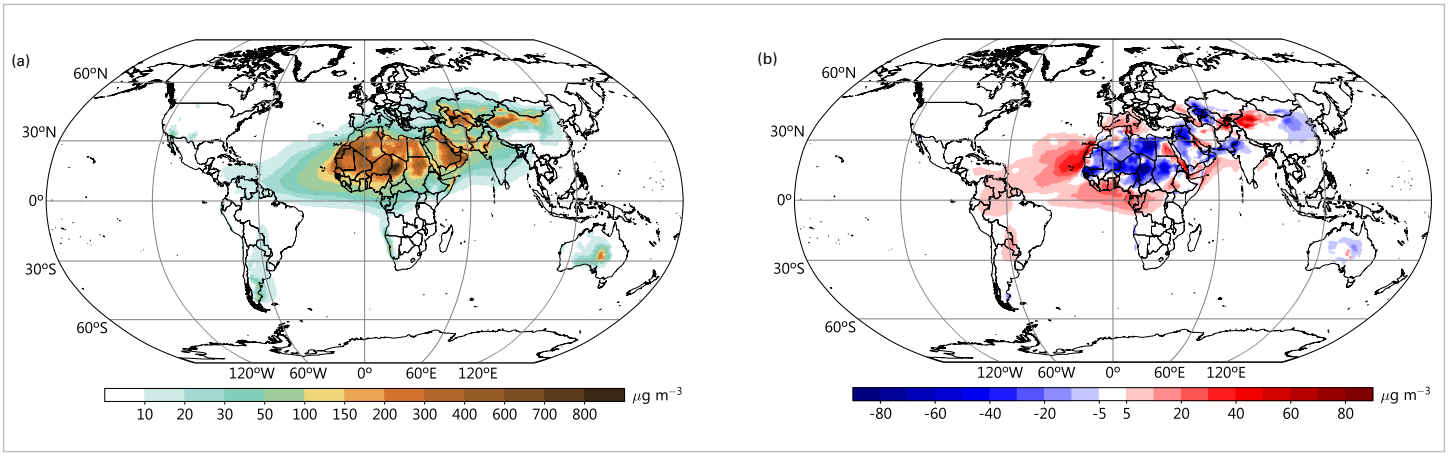

Figure 1. (a) Annual mean surface concentration of mineral dust (in μg m^{-3}) in 2024. (b) Anomaly of the annual mean surface dust concentration in 2024 relative to the 1981–2010 mean.

Source: These results are derived from the Modern-Era Retrospective Analysis for Research and Applications, Version 2 (MERRA-2) dataset. For more details on MERRA-2 see Gelaro et al. (2017). Third-party map. This map was provided by China Meteorological Administration (CMA) on 1 May 2025 and may not fully align with United Nations and WMO map guidance.

Europe, spanning Spain, the Mediterranean Sea and Italy; West Africa, covering the western Sahara Desert, Liberia, Côte d'Ivoire, Ghana, Togo, Benin, Cameroon, Gabon and the Congo; north-east Africa, including eastern Egypt, southern Sudan, and western Ethiopia; marine zones of the Red Sea and Arabian Sea; Central Asia, particularly Kazakhstan, Uzbekistan and Kyrgyzstan; north-western China; and the tropical Atlantic corridor between West Africa and the Caribbean.

In 2024, West Asia experienced intensified drought conditions and stronger wind patterns, both of which played key roles in the increased frequency and severity of sand and dust storms (SDS). Enhanced Shamal winds (June–August), driven by atmospheric pressure anomalies, along with springtime frontal systems, significantly contributed to dust mobilization, particularly in Syria and Iraq. As a result, populations in areas such as Kuwait, eastern Saudi Arabia, Iraq, eastern Syria, the southern Persian Gulf and southern Iran (from Khuzestan to the Sistan Basin) faced elevated exposure to SDS events.

Multiple environmental and human-induced factors contributed to the rise in dust emissions across the region. These include land use changes such as overgrazing and deforestation, suboptimal land and resource management, rapid urbanization and infrastructure expansion, reduced soil stability, and the drying of ecologically sensitive areas such as the Mesopotamian Marshes and Hammar Marshes in Iraq, and Lake Urmia in Iran.

Global aerosol reanalysis products (such as MERRA-2 in Figure 1, and Copernicus Atmosphere Monitoring Service (CAMS)) provide valuable insights into dust aerosol distributions, but they exhibit notable limitations over North America. These global products often underestimate local dust emissions due to outdated or coarse-resolution source inventories that fail to capture the complexity of regional dust sources such as dry lakebeds, agricultural lands and construction zones in the south-west United States of America. The consensus among aeolian scientists in North America is that 2024 was an average year when it came to sand and dust storms. The Southern High Plains (SHP) of Texas and the Chihuahua Desert (CD), just to the west and south-west of the SHP, form one of the largest contiguous dust sources in North America (Eibedingil et al., 2023). Records from a Texas Council on Environmental Quality (TCEQ) air quality station near downtown El Paso, Texas, indicated that the National Ambient Air Quality Standard (NAAQS) for particulate matter with a diameter less than 10 μm (PM_{10}) was exceeded four times during the months of February and March. High wind speeds, low relative humidity values and high carryover grass biomass from abundant rains the previous year resulted in seven wildfires in the SHP during late February and early March 2024. The largest of these wildfires, the Smokehouse Creek Fire, consumed over 1.1 million acres of grassland and many structures, and resulted in cattle and human deaths. With the protective cover of grasses burned, the resulting bare soil became a powerful source of dust during windy spring days, according to residents in the area. Additionally, the SHP and CD have been either abnormally dry or in a state of drought including exceptional drought, for much of the last two years. Webb et al. (2025) report, from a study conducted in this region, that aeolian sediment transport can increase by an order of magnitude with modest losses of surface vegetation. The analysis of specific events by region in this Bulletin highlights the localized consequences and responses to major sand and dust storms throughout the year.

Major sand and dust storm events in 2024

Canary Islands, December 2024

In December 2024, a dust outbreak was triggered by a high-pressure system over Algeria, which generated a Harmattan surge across a vast region of north-western Africa, in combination with a low-pressure system in the Atlantic, west of the Iberian Peninsula. This combination rapidly transported dust northward from the western Sahara Desert, reaching the Canary Islands. Such December outbreaks typically carry dust at lower altitudes, significantly impacting surface dust concentration levels where most of the population lives. In contrast, June-July-August outbreaks tend to transport dust at higher altitudes due to the intensified trade winds over the Canary Islands, with the altitude of the dust plume largely depending on the strength of the event. The vertical extension of dust affects how far it travels, and influences not only climate and weather, but also impacts air quality and human health.

Figure 2 presents a comparison between the NASA Micro Pulse Lidar (MPL) measurements from Santa Cruz de Tenerife (Spain) and the corresponding dust predictions from MONARCH. MONARCH is the reference forecast system of the WMO Barcelona Dust Regional Center. The concentration values at different altitudes align well between the vertical distribution observed by lidar and predicted by the model. Two dust layers – one extending from the surface to 1 800 m, and a second between 2 500 and 3 500 m – are shown by both the model and the lidar, reflecting a typical vertical distribution over the Canary Islands. Visibility data extracted from SYNOP bulletins further support these values, showing visibility ranging from 1 km at the surface to 20 km at an altitude of 2 300 m. Additionally, a daily maximum PM_{10} concentration of about 400 μg m^{-3}, measured at different air quality stations from the Cabildo de Tenerife network located up to 600 m above sea level, was in agreement with the lidar observations.

As of 26 July 2024, dust concentration profile predictions from MONARCH are available on the website of the WMO Barcelona Dust Regional Center. Information on the vertical distribution of dust concentration is highly

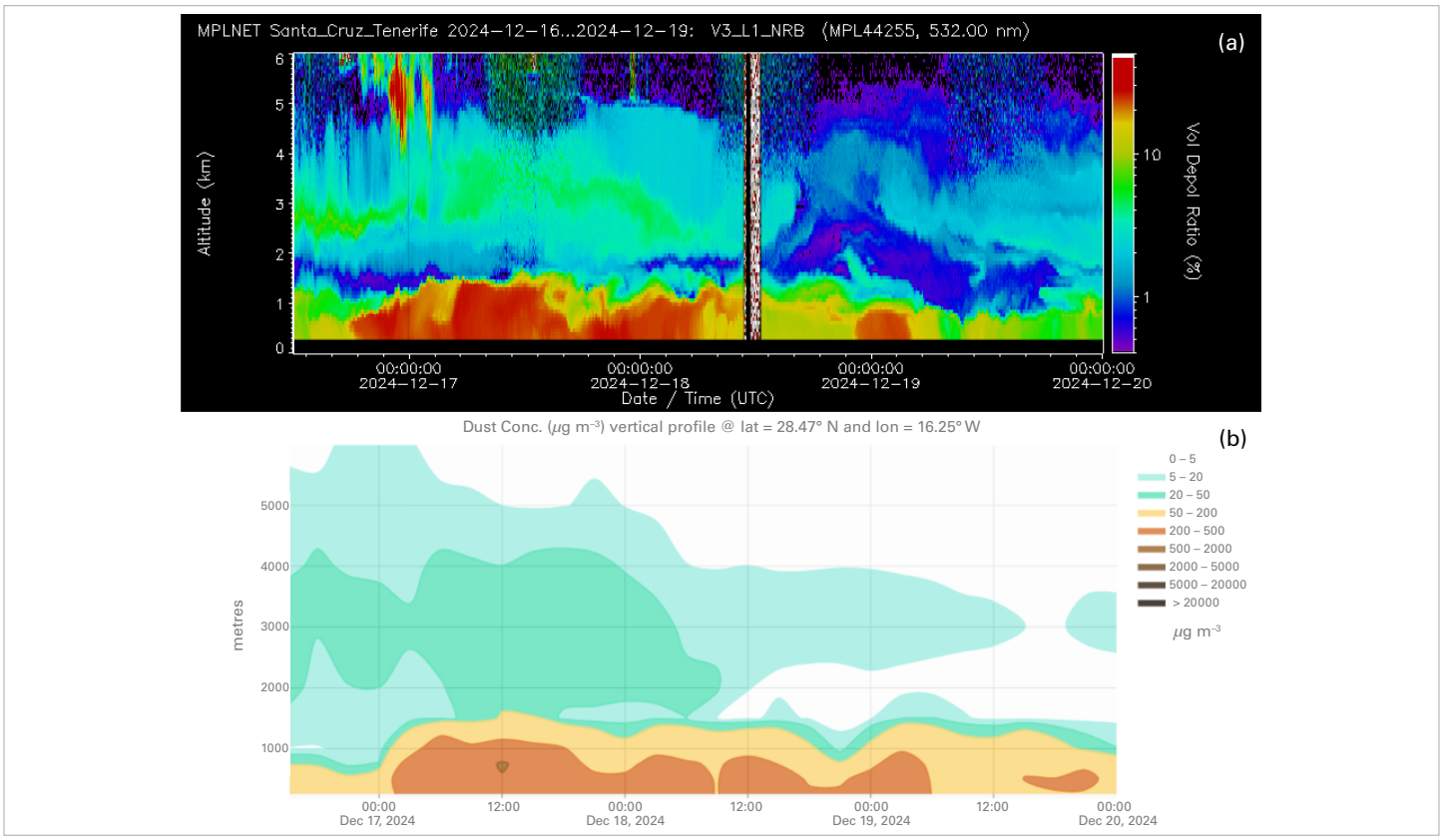

Figure 2. (a) Micro Pulse Lidar (MPL) measurements from Santa Cruz de Tenerife. (b) MONARCH vertical profile from 17 December 2024 to 20 December 2024.

Source: (a) NASA-MPLNet; (b) WMO Barcelona Dust Regional Center

valuable for weather forecasters, as it helps determine whether dust will affect surface dust concentration levels. The aviation sector is also significantly impacted by dust, and knowing the altitude of peak dust concentration along flight routes and near airports provides essential added value.

East Asia, June 2024

In 2024, East Asia experienced a total of 14 sand and dust weather events, 10 of which occurred in spring (March to May). From 27 to 29 March, extreme winds with maximum speeds exceeding 24 m/s struck eastern Mongolia and central Inner Mongolia, under the influence of a strongly developing Mongolian cyclone and a surface cold front. The fierce winds swept up large amounts of dust, transporting it south-eastward from southern Mongolia to densely populated regions such as the North China Plain and the Northeast China Plain (see Figure 3). Parts of central and eastern Inner Mongolia experienced severe sandstorms, with peak PM_{10} concentrations exceeding 5 000 $\mu g\ m^{-3}$. In the early hours of 28 March, affected by the dust weather, Beijing recorded a peak PM_{10} concentration of over 1 000 $\mu g\ m^{-3}$, and visibility dropped to 1 km.

Notably, from 21 to 24 June, northern China, including Beijing, was hit by another sand and dust event. This was a relatively rare occurrence, as sand and dust weather affecting central and eastern China in midsummer is uncommon. The primary cause was the poor vegetation growth in southern Mongolia and the Onqin Daga Sandy Land due to high temperatures and drought in late spring and early summer. Influenced by a slowly eastward-moving Mongolian cyclone, strong winds lifted multiple waves of dust and continuously transported them southward, causing Beijing's PM_{10} concentration to exceed 600$\mu g\ m^{-3}$. This event drew public attention to the increasing occurrence of summer dust storms driven by extreme weather in a changing climate.

West Asia, December 2024

Between 14 and 16 December 2024, an exceptional wintertime dust storm significantly affected extensive parts of West Asia, notably Iraq, Kuwait, Qatar and the Arabian Peninsula. This dust event had substantial socioeconomic consequences. It resulted in extensive disruptions to activities, including the cancellation of numerous flights, the widespread closure of schools and the postponement of public and outdoor events.

The dust storm began early on 14 December and continued to severely impact downwind cities for more than 48 hours. Within this period, the dust storm affected an extensive area exceeding 650 000 km^2. Air quality deteriorated dramatically, with surface dust concentrations reaching extraordinarily high values, surpassing 5 000 $\mu g\ m^{-3}$ in several locations

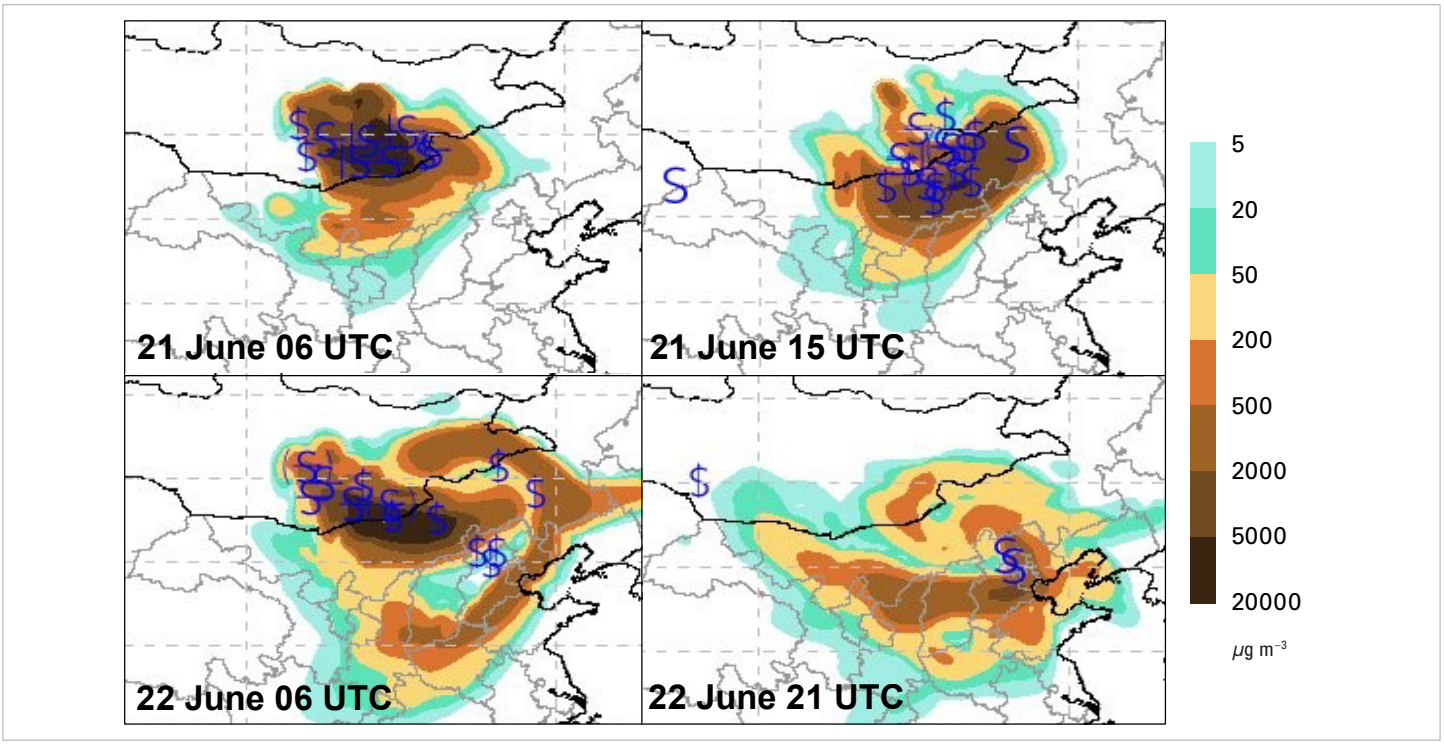

Figure 3. Comparison between observed SDS phenomenon (based on the visibility report, blue symbols indicate the weather stations where dust was recorded) and forecasted surface dust concentrations (μg m^{-3}) by CMA forecasting system on 21 and 22 June 2024

Source: Third-party map. This map was provided by the WMO Beijing Dust Forecast Center on 3 July 2025 and may not fully align with United Nations and WMO map guidance.

(Figure 4). Consequently, visibility reduced drastically, often dropping below 1 km over vast portions of the affected regions. Cities closer to the dust source, such as Salah Ad Din (Iraq), Baghdad and Kuwait City, experienced significantly higher dust concentrations compared to distant locations like Abu Dhabi, where dust concentrations were notably lower. Originating primarily from north-west Iraq and north-east Syria, the event was characterized by a distinctive and rare synoptic-scale meteorological condition in the region. The event was driven by atypical jet stream dynamics and significant topographic interactions.

Ongoing research

Remote-sensing-based identification of spring dust intensity

The advancement of more precise remote-sensing inversion technology for dust aerosols has long been a hot topic in the atmospheric environment field. Gridded observation data of dust intensity level remains a gap in current dust monitoring and forecasting operations. Based on the Himawari-9 geostationary satellite data, a recent study (Jiang et al., 2024), establishes a new method

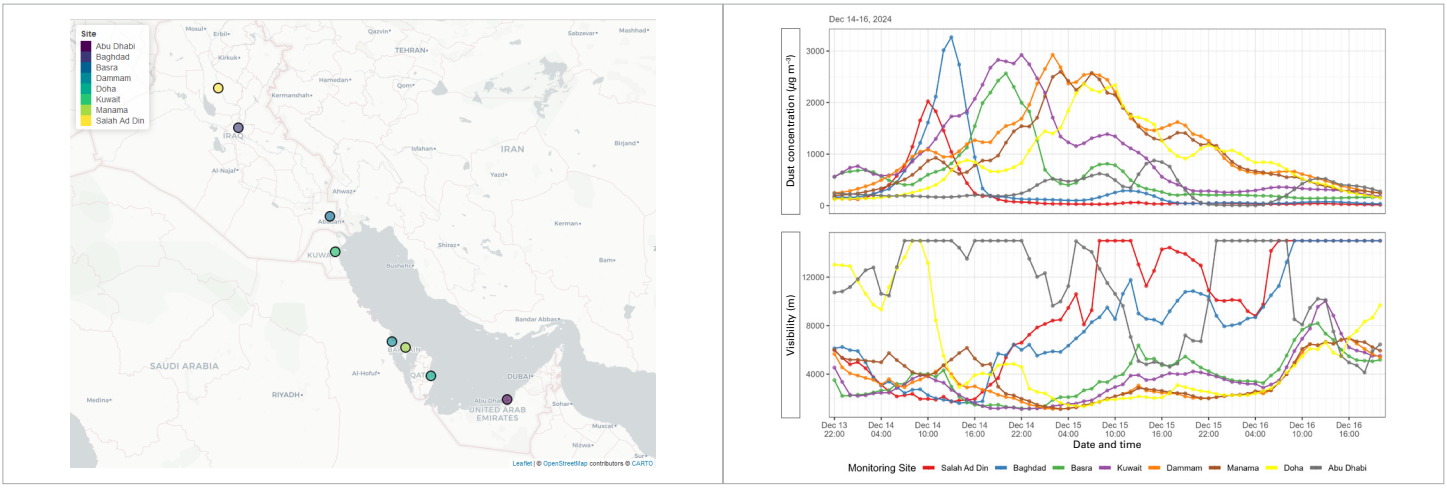

Figure 4. (a) Geographic locations of major cities affected by the 14–16 December 2024 dust storm. (b) Time series of surface dust concentrations (μg m^{-3}) observed across selected West Asian cities.

Source: Third-party map. This map was provided by the WMO Jeddah Dust Regional Center on 3 July 2025 and may not fully align with United Nations and WMO map guidance.

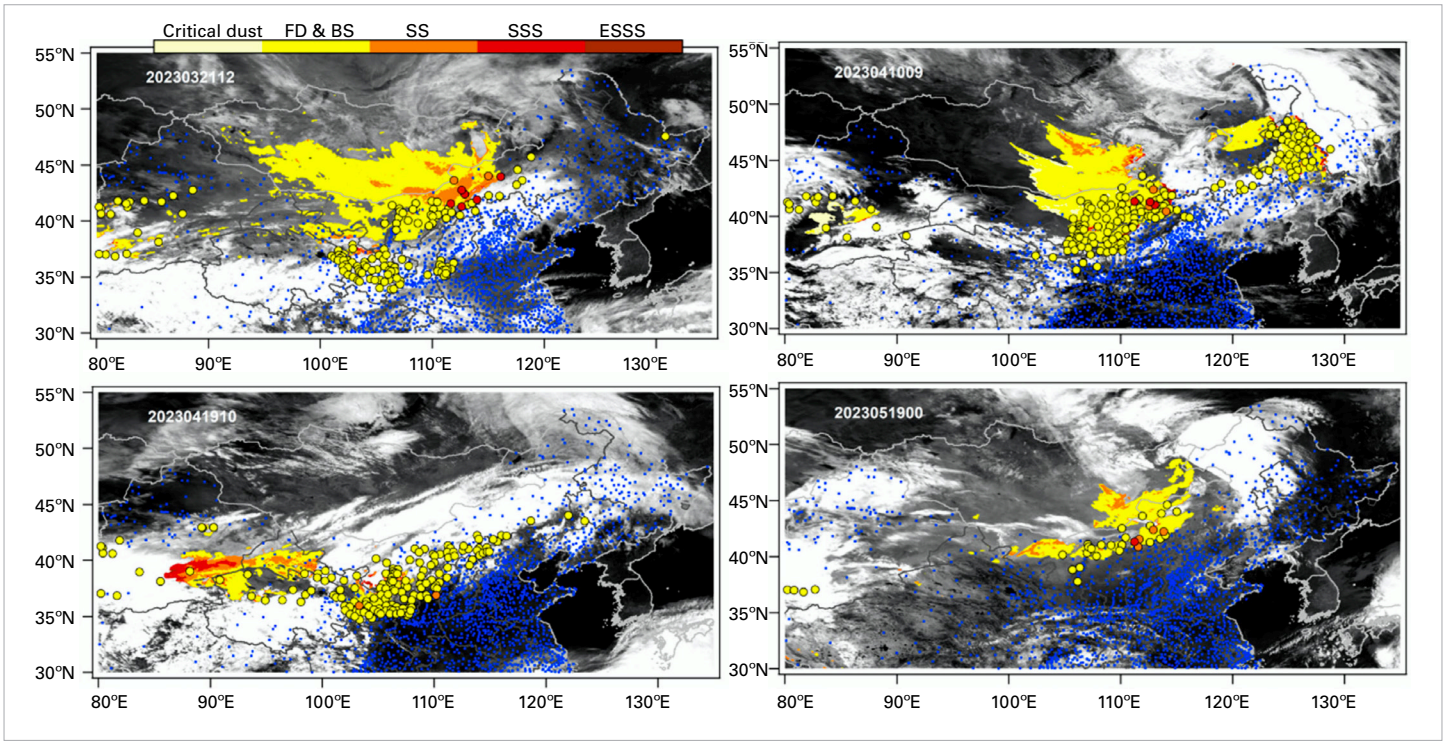

Figure 5. Comparison of satellite identification results of dust level with near-surface station observations at 1200 UTC on 21 March (upper left), 0900 UTC on 10 April (upper right), 1000 UTC on 19 April (lower left) and 0000 UTC on 19 May 2023 (lower right). The black and white backgrounds of the figures represent the cloud images at the corresponding time. The blue dots denote the distribution of ground observation stations. FD = floating dust; BS = blowing sand; SS = sand storm; SSS = severe sand storm; ESSS = extremely severe sand storm.

Source: Third-party map. This map was taken from Jiang et al. (2024) on 1 May 2025 and may not fully align with United Nations and WMO map guidance.

for identifying spring dust events. This method takes into account how different surfaces on the ground – such as deserts or cities – affect the satellite's readings. By checking background brightness temperature differences from space several times a day, the method entails looking for patterns that match dust levels measured on the ground. This helps create a reliable way to estimate the intensity of dust conditions near the surface. The results of the application of this method (see Figure 5) indicate that the algorithm can effectively identify the presence or absence of dust, with a misjudgement rate of less than 3%. With regard to dust intensity, the identification of blowing sand and floating dust aligns relatively well with ground-based observations, but notable uncertainties exist in determining their intensity for extreme events. Two important error sources in the dust identification results of this study are: firstly, the differences between ground-based observations and satellite identification caused by non-grounded dust in the upper air and; secondly, the selection of dust identification thresholds.

Real-time mapping of gapless 24-hour surface PM_{10}

Large-scale mapping of surface PM_{10} concentration remains a key focus for sand and dust storm monitoring. Satellite aerosol optical depth (AOD)-based data fusion approaches effectively decouple the non-linear AOD–PM_{10} relationship, facilitating high-resolution PM_{10} data acquisition. However, these methods are constrained by spatial incompleteness and the absence of night-time data. Zhang et al. (2025) introduced a gridded visibility-based real-time surface PM_{10} retrieval (RT-SPMR) framework for China. This framework utilizes multisource data inputs, with gridded visibility serving as a key variable (Zhang et al., 2024a) and employs dynamically updated machine-learning models to produce 24-hour PM_{10} data on a 6.25-km grid.

Taking the record-breaking dust storm that occurred in March 2021 as an example, the RT-SPMR model demonstrated its efficacy in tracking the fine-scale evolution of the dust intrusion process, especially in under-observed areas (Figure 6). As a result, the operational RT-SPMR framework offers a comprehensive real-time capability for monitoring PM_{10} pollution in China and holds significant potential for enhancing the accuracy of dust storm forecasting models by improving the PM_{10} initial field.

Global distribution of scattering and absorbing dust retrieved from AERONET observations

The Aerosol Robotic Network (AERONET, https://aeronet.gsfc.nasa.gov/), a global network of sun photometers, has been offering consistent measurements of aerosol optical properties across diverse environments for more than 30 years. Scientists around the world have used AERONET data to study aerosol characteristics in specific locations and on a global scale. By analysing how light behaves when it passes through these particles, researchers have been able to identify different types of aerosols and estimate how much of each type is

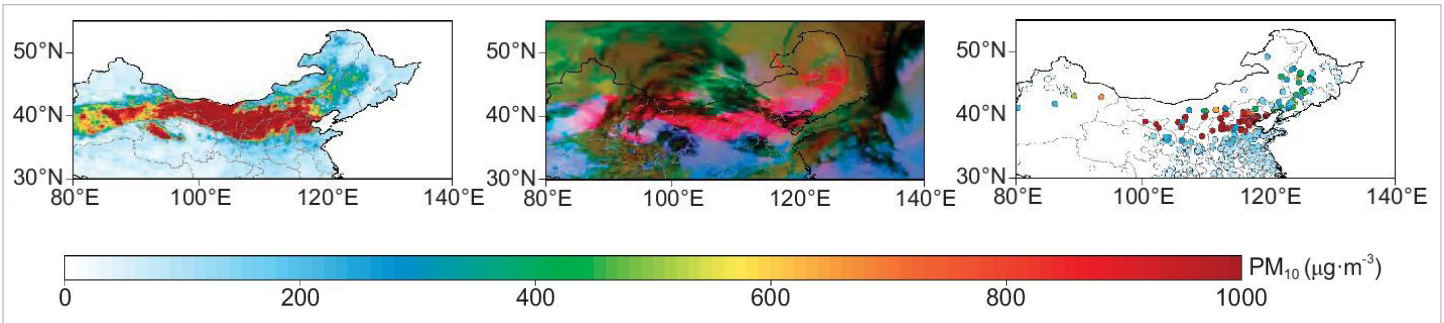

Figure 6. Tracking a large-scale dust storm incursion process using gapless PM_{10} from a gridded visibility-based real-time surface PM_{10} retrieval (RT-SPMR) model. The dust plumes, as revealed by gapless PM_{10} retrievals (on the left), Himawari-8 dust RGB composite images (in the centre), and PM_{10} observations (on the right) at 1600 CST (China standard time) on 15 March 2021.

Source: Third-party map. This map was taken from Zhang et al. (2025) on 1 May 2025 and may not fully align with United Nations and WMO map guidance.

present in the air. International cooperation activities are fundamental to support long-term measurements. As an example, the official scientific cooperation between Spain and Cuba for over 15 years has been supporting observations, know-how transfer and joint research on aerosol optical properties in Cuba. Antuña-Marrero et al. (2025) describe the origin, evolution, obstacles and scientific results achieved from this cooperation. The first step was setting up, in 2007 in Camagüey in the east of Cuba, in situ PM measurements. Later, in 2008, a CIMEL sun photometer was installed in the same location. The data from Camagüey, combined with the data of AERONET stations in Ragged Point (Barbados), Guadeloupe and La Parguera (Puerto Rico), have made it possible to determine the climatology of the aerosol optical properties in the Caribbean Islands (see Rodríguez Vega et al., 2022).

To better understand the aerosol impacts on climate and weather, researchers look at specific features such as how much light the particles absorb or scatter, and the size of the particles. Some earlier methods estimated the amount of each aerosol component using certain optical properties from AERONET data, but these estimates could sometimes be inaccurate.

A recent study (Zhang et al., 2024b), used a new component inversion approach which can directly retrieve aerosol component concentration from AERONET radiance and spectral AOD measurements. This method has been developed in the framework of the Generalized Retrieval of Atmosphere and Surface Properties (GRASP)/Component retrieval algorithm, which enables detailed aerosol composition analysis. The study analysed data collected from 191 AERONET sites between 2012 and 2021. The aim was to characterize the spatial and temporal variability of key aerosol components, including dust, black carbon, organic matter and sulfates, and to assess their respective roles in aerosol radiative effects. The absorbing (mainly iron oxides) and scattering dust are primarily distributed in regions such as the Sahara Desert, West Asia and South Asia (shown in Figure 7(a) and (b)).

The Sahara remains the world's largest source of atmospheric dust, with annual columnar concentrations exceeding 1 580 mg/m² (scattering) and 20 mg/m² (absorbing) at sites such as Cinzana (Mali), Banizoumbou (Niger), and Dakar (Senegal). During June-July-August (JJA), these concentrations increase notably, reaching over 2 700 mg/m² (scattering) and 50 mg/m² (absorbing) at Cinzana and Banizoumbou, accounting for 1.8%–2.0% of total dust.

High dust levels are also recorded in South and West Asia, with values of 1 761 mg/m² at Pune (India) and 1 523 mg/m² at Mezairaa (UAE). South Asia shows strong seasonal variation, with dust peaking in JJA and a secondary peak in September-October-November (SON). Kanpur (India) sees scattering dust up to 2 530 mg/m² in JJA, while Jaipur (India) records absorbing dust at 22.6 mg/m². In contrast, East Asia peaks in March-April-May (MAM), with values reaching 1 600 mg/m² (scattering) and 11 mg/m² (absorbing) at Beijing. In West Asia, peak concentrations in JJA exceed 1 800 mg/m² in Kuwait and Mezairaa (UAE), while December-January-February (DJF) shows minimal activity, namely 1.1 mg/m² absorbing dust at Sede Boker (Israel). In contrast, continental Europe, North and South America have much lower dust levels. North America receives Saharan dust in JJA via tropical easterlies. The Amazon basin receives significant African dust, mainly from the Bodélé Depression, throughout the year, supporting rainforest ecosystems. These plumes take 7–10 days to arrive and interact with marine aerosols, biomass burning, and local deforestation emissions, contributing to stable coarse-mode aerosol patterns. Regional differences in dust mineralogy play a critical role in determining absorption and scattering properties. For example, North African dust often contains high concentrations of iron-rich minerals like hematite, which enhance absorption and reduce reflectivity, especially in the visible spectrum. In contrast, dust from regions like Central Asia or Australia tends to be dominated by lighter silicates such as quartz and feldspar, leading to higher scattering and lower absorption. These mineralogical variations across source regions highlight the importance of region-specific dust characterization.

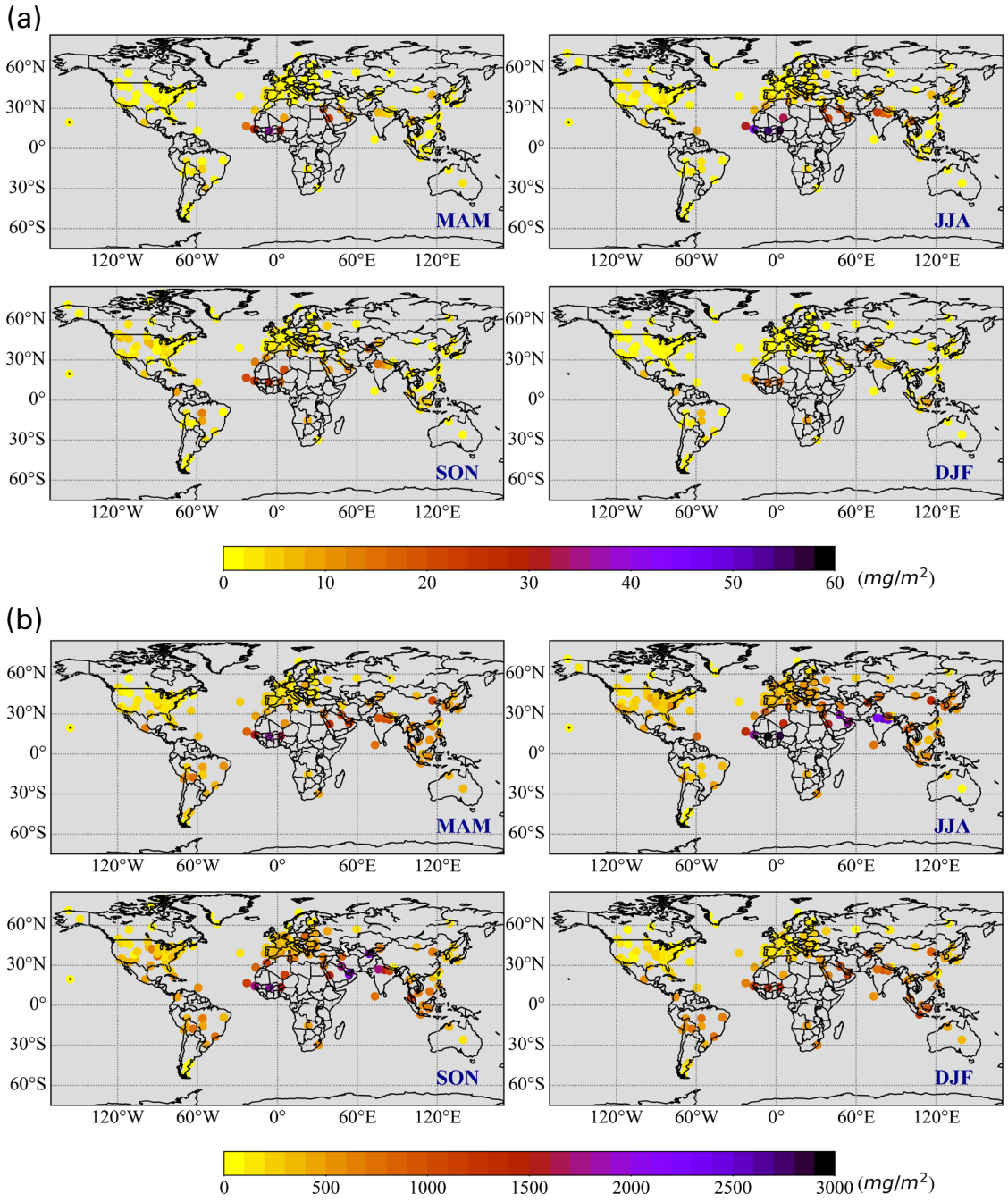

Figure 7. Seasonal spatial distribution of (a) absorbing dust and (b) scattering dust column mass concentration (mg/m^2) derived from AERONET observations at 191 sites using the GRASP/Component approach for the period 2012–2021

Source: Third-party map. This map was taken from Zhang et al. (2024b) on 1 June 2025 and may not fully align with United Nations and WMO map guidance.

First modelled global dust mineralogy results using the NASA-EMIT source map

Minerals in atmospheric dust play a crucial role in shaping its interaction with relevant components of the Earth system. Iron oxides, such as hematite and goethite, absorb short-wave radiation (Sokolik ant Toon, 1999; Di Biagio et al., 2019), influencing the Earth's energy balance, while quartz or K-feldspars act as efficient ice nuclei (Atkinson et al., 2013; Harrison et al., 2019), contributing to the formation of mixed-phase clouds. Iron- and phosphorus-bearing minerals carry essential nutrients to terrestrial and marine ecosystems (Mahowald et al., 2009; Yu et al., 2015), while other minerals, like calcite, affect aerosols' acidity and intervene in atmospheric chemistry processes. Incorporating these complex effects into Earth System Models (ESMs), fundamental for climate assessments, remains a challenge due to our limited knowledge about the mineralogy of dust sources and its particle size distribution at emission (see, for example, Gonçalves Ageitos et al., 2023; Obiso et al., 2024; Song et al., 2024).

ESMs have until now relied on soil mineralogy atlases created by extrapolating a limited set of observations. The high-resolution spaceborne NASA Earth Surface Mineral Dust Source Investigation Imaging Spectrometer (EMIT) allows the generation of

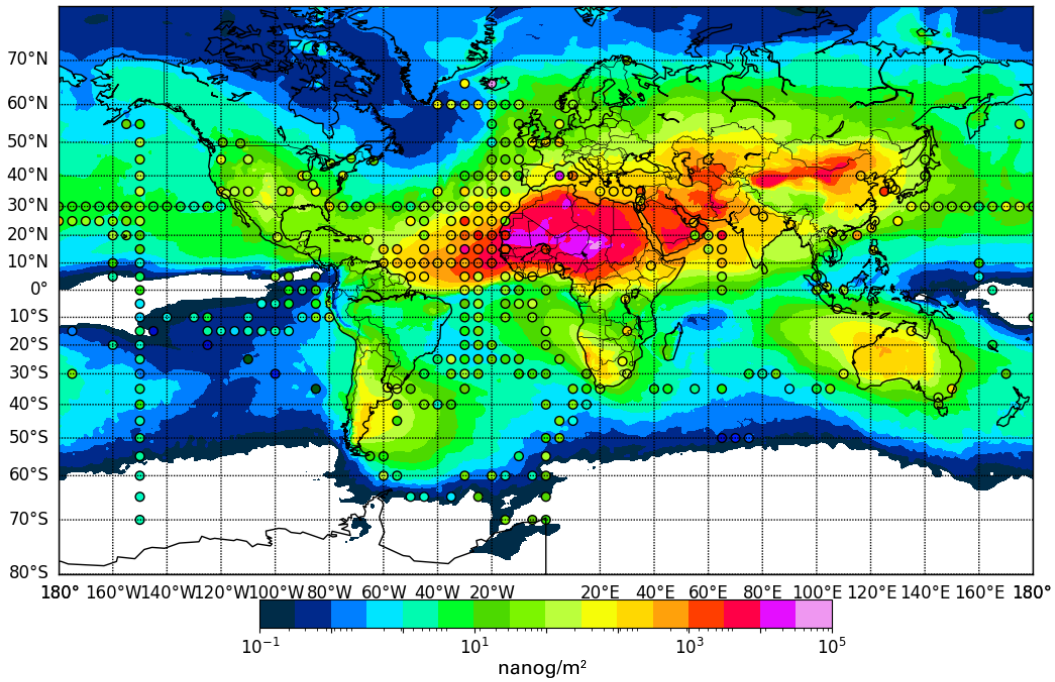

Figure 8. Simulated 2019 iron in $PM_{2.5}$ in ng m^{-3} versus observations from SPARTAN (https://www.spartan-network.org/data), as well as against climatological observations of iron surface concentration gathered by Myriokefalitakis et al. (2018)

Source: Third-party map. This map was provided by ECMWF on 1 May 2025 and may not fully align with United Nations and WMO map guidance.

observationally-constrained soil mineral abundance maps at the global scale (Green et al., 2020; Thompson et al., 2023; Mahowald et al., 2024).

The first version of the map has been adopted as a source descriptor in four different ESMs with explicit mineralogy representation. These include MONARCH (Klose et al., 2021, and references therein) and the Integrated Forecasting System (IFS-COMPO) of the European Centre for Medium-Range Weather Forecasts (ECMWF) (Rémy et al., 2022). MONARCH is the reference forecast system of the WMO Barcelona Dust Regional Center and IFS-COMPO is core to the Copernicus Atmosphere Monitoring Service (CAMS).

A set of MONARCH simulations, constrained with reanalyses, shows improvements with respect to analogous simulations performed with previous soil atlases, particularly in the characterization of iron oxides and calcite per region.

Figure 8 shows a comparison of IFS-COMPO-simulated iron in $PM_{2.5}$ and observations from the Surface Particulate Matter Network (SPARTAN), as well as climatological observations of iron surface concentration. This extended version of the CAMS system is now being used to create a long-term dataset (2003–2026), with an improved dust emission scheme developed in the Horizon Europe CAMS Aerosol Advancement (CAMAERA) project and without data assimilation of atmospheric composition. The output will be simulated 3-hourly emission, concentration, deposition and burden of 12 mineralogical species, which will be made available to the scientific community and the general public through the CAMS Atmosphere Data Store (https://ads.atmosphere.copernicus.eu/).

Other news

United Nations sand and dust storms decade

On 10 July 2024, the United Nations General Assembly officially proclaimed 2025–2034 as the United Nations Decade on Combating Sand and Dust Storms, by consensus. The relevant resolution mandates the United Nations Secretary-General to coordinate global, regional and national efforts over these ten years, focusing on preventing, halting and mitigating the adverse impacts of sand and dust storms. The resolution emphasizes reliance on voluntary funding, including from the private sector. Implementation is designed to be highly collaborative, leveraging the United Nations Coalition on Combating Sand and Dust Storms to facilitate shared early warning systems, science-based guidance, sustainable land management and afforestation efforts.

Launch of EarthCARE satellite and its application to airborne dust monitoring

The Earth Cloud Aerosol and Radiation Explorer (EarthCARE) is a satellite mission developed by the European Space Agency (ESA) and the Japan Aerospace Exploration Agency (JAXA). The EarthCARE satellite was launched on 28 May 2024, at 2220 UTC. Its four scientific instruments, onboard a single platform, are an atmospheric lidar (ATLID), a cloud profiling radar (CPR) with Doppler capability, a multi-spectral imager (MSI) and a broadband radiometer (BBR). The homogeneous global scale aerosol vertical profile dataset from EarthCARE with, in synergy with ground-based observations and numerical models, is expected to enhance our

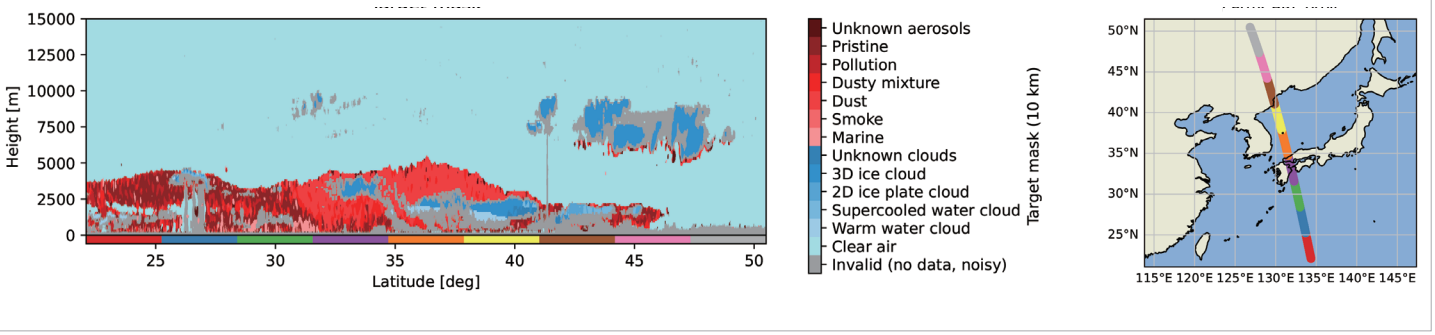

Figure 9. Vertical distribution of aerosol and clouds over the Sea of Japan and the East China Sea on the 25 March 2025 night-time overpass by ATLID (left). Dust corresponds to red colours. The EarthCARE Orbit is indicated in the right panel.

Source: Third-party map. This map was provided by the Earth Observation Research Center, Japan Aerospace Exploration Agency (JAXA) on 1 May 2025 and may not fully align with United Nations and WMO map guidance.

understanding of long-range transport of airborne dust and changes in altitude during transport. It is expected to contribute to climate and health impact assessments. The EarthCARE data products are publicly available and can be downloaded for free (https://gportal.jaxa.jp/gpr/?lang=en).

Dust storms in the Gobi and Taklamakan Deserts in Asia mainly occur in the spring (March to May) and can reach the upper troposphere. Sometimes, this dust is carried eastward over the ocean by the westerly winds, a phenomenon known as "yellow sand" in Japan. On 25 March 2025, the Japan Meteorological Agency (JMA) reported the first yellow sand event of the year in Tokyo. The ATLID observed the vertical distribution of the associated dust plume over the Sea of Japan and the East China Sea, as shown in Figure 9. The target mask, which classifies aerosols and clouds, is included in the Level 2 product called ATL_CLA.

A multi-reanalysis consensus indicator for tracking sand and dusts storm health risks

Drought, poor land management and the expansion of wildfire-burned areas are contributing to a rising risk of SDSs. The Dust Reanalysis Working Group, coordinated by the WMO Sand and Dust Storm Warning Advisory and Assessment System (SDS-WAS), has developed a dust and sand storm indicator for the public health sector in collaboration with the World Health Organization (WHO). This indicator uses a state-of-the-art multi-reanalysis consensus to estimate mineral dust concentrations in PM_{10} ("dust-PM_{10}") from arid and semi-arid regions, combined with population data to assess human exposure. Globally, during 2018–2022, approximately 3.8 billion people – 48.9% of the world's population – were exposed to average annual concentrations of dust-PM_{10} exceeding the WHO's recommended annual threshold of 15 $\mu g\ m^{-3}$ for total PM_{10}. This represents a 31% increase, from 2.9 billion people (44.5%) during 2003–2007.

Between 2003–2007 and 2018–2022, the number of days in which people were exposed to very dangerous levels of dust-PM_{10} (>45 $\mu g\ m^{-3}$) increased in 42% of countries and decreased in 36%. Exposure varied widely, from only a few days in relatively unaffected areas to more than 87% of days – equivalent to over 1 600 days in five years – in the most dust-prone regions. Notably, two-thirds of the countries experiencing higher levels of mineral dust exposure fall into the high or very high Human Development Index (HDI) categories, while 47% of countries with lower exposure are classified as low or medium HDI. This indicator and the associated findings were published in the *The 2024 Report of the Lancet Countdown on Health and Climate Change* (Romanello et al., 2024).

The economic impact of sand and dust storms on the USA

A recent assessment of the economic impact of dust and wind erosion on the USA (see Feng et al., 2025) suggests that the impacts of dust and wind erosion are often under-estimated. This study estimated that they cost 154.4 billion US dollars (US$) in 2017 – more than a fourfold increase over the 1995 calculation. The Feng et al. (2025) estimate included costs to households, cropland agriculture, wind and solar energy, mortality from fine dust exposure, health costs due to Valley fever (an infectious disease caused by the soilborne fungus *Coccidioides*), motor vehicle transportation and mitigation of dust "hotspots". While the costs of dust related to cropland agriculture appear to have declined, the economic burden on the other analysed sectors has increased, most of them greatly. The actual cost could be much higher than the estimated US$ 154.4 billion, since reliable national-scale evaluations of many of dust's other economic impacts (for example, on human morbidity, the hydrological cycle, aviation and rangeland agriculture) were not available. Even without these unaccounted effects, the authors' estimation of the disaster costs of wind erosion and dust in 2017 emphasizes that they can be of the same magnitude as other meteorological and geophysical phenomena. The study brings the need for more quantitative research into dust's economic cost in many sectors of the economy and suggests that investment in dust mitigation and wind erosion control would reap large returns.

Figure 10. Group picture taken during the first International Conference on Sand and Dust Storms in Riyadh, Saudi Arabia. Participants included Slobodan Nickovic (Vice-Chair of the Global Steering Committee), the four chairs of the SDS-WAS Regional Nodes (Ana Vukovic Vimic for North Africa, the Middle East and Europe; Takashi Maki for Asia; Andrea Sealy for the Americas; and Jumaan Alqahtani for the Gulf Cooperation Council), as well as Sara Basart and Hesham Abdel Ghany (WMO).
Photo credit: NCM

Sand and dust storm international events in Saudi Arabia

The first International Conference on Sand and Dust Storms took place in Riyadh, Saudi Arabia, from 4 to 6 March 2024. It was organized by the National Center for Meteorology (NCM), Saudi Arabia, which also hosts one of the WMO SDS-WAS Regional Centres for the Gulf Cooperation Council region. A broad international representation of researchers and forecasters was present, and the event included discussions on, among other topics, monitoring and predictive modelling, dust and climate interactions, health impacts and mitigation strategies. Representatives of the WMO SDS-WAS Global Steering Committee attended the event (see Figure 10).

It is fitting that the thirtieth anniversary of the United Nations Convention to Combat Desertification (UNCCD) was celebrated in Riyadh at the 16th meeting of the Conference of the Parties (COP16) on 2–13 December 2024. When the Convention was established in June 1994, parties made a promise to the world that they would combat desertification and mitigate the impacts of drought that have devastating effects on peoples' lives across the world, including sand and dust storms. Within the programme of the event, Resilience Day on 10 December aimed to address the critical issues of building planetary and societal resilience in the face of a changing climate, land degradation, droughts and SDSs. The plenary sessions were organized by the World Bank and WMO. The United Nations Coalition on Combating SDS also organized an SDS-dedicated event (Figure 11 right). Additionally, on 4 December, a dedicated side event on SDSs was jointly organized by the NCM and WMO, with the participation of the WMO SDS-WAS Global Steering Committee (see Figure 11 left). During the side event, Dr Ayman Salem Ghulam (Permanent Representative of the Kingdom of Saudi Arabia to WMO) announced financial support from Saudi Arabia amounting to up to US$ 10 million over the next five years, to enhance early warning systems for sand and dust storms.

Figure 11. (Left) Group photo during the UNCCD COP16 SDS side event on 4 December in Riyadh. From left to right: Takashi Maki, Jumaan Alqahtani, Daniel Tong, Dr Ayman Salem Ghulam (Chief Executive Officer, NCM and Permanent Representative to WMO), Ana Vukovic Vimic, Sara Basart (WMO) and Andrea Sealy. (Right) Resilience Day plenary session at the UNCCD COP16 SDS side event on 10 December in Riyadh. Carol Chouchani Cherfane (United Nations Economic and Social Commission for Western Asia (ESCWA)) introducing the panellists of the session "Promote Early Warning Systems".
Photo credit: WMO

References

Atkinson, J. D.; Murray, B. J.; Woodhouse, M. T. et al. The Importance of Feldspar for Ice Nucleation by Mineral Dust in Mixed-phase Clouds. *Nature* **2013**, *498*, 355–358. DOI: 10.1038/nature12278.

Di Biagio, C.; Formenti, P.; Balkanski, Y. et al. Complex Refractive Indices and Single-scattering Albedo of Global Dust Aerosols in the Shortwave Spectrum and Relationship to Size and Iron Content. *Atmospheric Chemistry and Physics* **2019**, *19*, 15503–15531. https://doi.org/10.5194/acp-19-15503-2019.

Eibedingil, I. G.; Gill, T. E.; Kandakji, T. et al. Effect of Spatial and Temporal "Drought Legacy" on Dust Sources in Adjacent Regions. *Land Degradation And Development* **2023**, *35*, 1511–1525. https://doi.org/10.1002/ldr.5002.

Feng, I. Y.; Gill, T. E.; Van Pelt, R. S. et al. Economic Costs of Wind Erosion in the United States. *Nature Sustainability* **2025**, *8*, 307–314. https://doi.org/10.1038/s41893-024-01506-4.

Gelaro, R. Status and Plans for Reanalysis at NASA/GMAO. *International Conference on Reanalysis*, Rome, 13-17 November 2017. https://ntrs.nasa.gov/citations/20170011574.

Gonçalves Ageitos, M.; Obiso, V.; Miller, R. L. et al. Modeling Dust Mineralogical Composition: Sensitivity to Soil Mineralogy Atlases and Their Expected Climate Impacts. *Atmospheric Chemistry and Physics* **2023**, *23*, 8623–8657. https://doi.org/10.5194/acp-23-8623-2023.

Green, R. O.; Mahowald, N.; Ung, C. et al. The Earth Surface Mineral Dust Source Investigation: An Earth Science Imaging Spectroscopy Mission. *IEEE Aerospace Conference*, Big Sky, USA, 1–14 March 2020; IEEE. https://doi.org/10.1109/AERO47225.2020.9172731.

Harrison, A. D.; Lever, K.; Sanchez-Marroquin, A. et al. The Ice-nucleating Ability of Quartz Immersed in Water and its Atmospheric Importance Compared to K-feldspar. *Atmospheric Chemistry and Physics* **2019**, *19*, 11343–11361. https://doi.org/10.5194/acp-19-11343-2019.

Jiang, Q.; An, L.; Wang, F. et al. Identification Method for Spring Dust Intensity Levels Based on Multiple Remote Sensing Parameters. *Remote Sensing* **2024**, *16*. https://doi.org/10.3390/rs16142606.

Klose, M.; Jorba, O.; Gonçalves Ageitos, M. et al. Mineral Dust Cycle in the Multiscale Online Nonhydrostatic AtmospheRe CHemistry Model (MONARCH) Version 2.0. *Geoscientific Model Development* **2021**, *14*, 6403–6444. https://doi.org/10.5194/gmd-14-6403-2021.

Mahowald, N. M.; Engelstaedter, S.; Luo, C. et al. Atmospheric Iron Deposition: Global Distribution, Variability, and Human Perturbations. *Annual Review of Marine Science* **2009**, *1*, 245–278. https://doi.org/10.1146/annurev.marine.010908.163727.

Mahowald, N.; Li, L.; Miller, R. et al. *EMIT L4 Earth System Model Products V001* [dataset]. NASA EOSDIS Land Processes Distributed Active Archive Center, 2024. https://doi.org/10.5067/EMIT/EMITL4ESM.001.

Myriokefalitakis, S.; Ito, A.; Kanakidou, M. et al. Reviews and Syntheses: The GESAMP Atmospheric Iron Deposition Model Intercomparison Study. *Biogeosciences* **2018**, *15*, 6659–6684. https://doi.org/10.5194/bg-15-6659-2018.

Obiso, V.; Gonçalves Ageitos, M.; Pérez García-Pando, C. et al. Observationally Constrained Regional Variations of Shortwave Absorption by Iron Oxides Emphasize the Cooling Effect of Dust. *Atmospheric Chemistry and Physics* **2024**, *24*, 5337–5367. https://doi.org/10.5194/acp-24-5337-2024.

Rémy, S.; Kipling, Z.; Huijnen, V. et al. Description and Evaluation of the Tropospheric Aerosol Scheme in the Integrated Forecasting System (IFS-AER, Cycle 47R1) of ECMWF. *Geoscientific Model Development* **2022**, *15*, 4881–4912. https://doi.org/10.5194/gmd-15-4881-2022.

Rodríguez Vega, A.; Antuña-Marrero, J. C.; Barriopedro, D. et al. Climatology of Aerosols over the Caribbean Islands: Aerosol Types, Synoptic Patterns, and Transport. *Journal of Applied Meteorology and Climatology* **2022**, *61*, 369–391. https://doi.org/10.1175/JAMC-D-21-0015.1.

Romanello, M.; Walawender, M.; Hsu, S.-C. et al. The 2024 Report of the Lancet Countdown on Health and Climate Change: Facing Record-breaking Threats from Delayed Action. *The Lancet* **2024**, *404* (10465), 1847–1896. DOI: 10.1016/S0140-6736(24)01822-1.

Sokolik, I. N.; Toon, O. B. Incorporation of Mineralogical Composition into Models of the Radiative Properties of Mineral Aerosol from UV to IR Wavelengths. *Journal of Geophysical Research: Atmospheres* **1999**, *104*, 9423–9444. https://doi.org/10.1029/1998JD200048.

Song, Q.; Ginoux, P.; Gonçalves Ageitos, M. et al. Modeling Impacts of Dust Mineralogy on Fast Climate Response. *Atmospheric Chemistry and Physics* **2024**, *24*, 7421–7446. https://doi.org/10.5194/acp-24-7421-2024.

Thompson, D. R.; Green, R. O.; Bradley, C. et al. On-orbit Calibration and Performance of the EMIT Imaging Spectrometer. *Remote Sensing of Environment* **2024**, *303*. https://doi.org/10.1016/j.rse.2023.113986.

Webb, N. P.; Wheeler, B.; Edwards, B. L. et al. Magnitude Shifts in Aeolian Sediment Transport Associated with Degradation and Restoration Thresholds in Drylands. *Journal of Geophysical Research: Biogeosciences* **2025**, *130*. https://doi.org/10.1029/2024JG008581.

Yu, H.; Chin, M.; Yuan, T. et al. The Fertilizing Role of African Dust in the Amazon Rainforest: A First Multiyear Assessment Based on Data from Cloud-Aerosol Lidar and Infrared Pathfinder Satellite Observations. *Geophysical Research Letters* **2015**, *42*, 1984–1991. https://doi.org/10.1002/2015GL063040.

Zhang, X.; Gui, K.; Zeng, Z. et al. Mapping the Seamless Hourly Surface Visibility in China: A Real-time Retrieval Framework Using a Machine-learning-based Stacked Ensemble Model. *Climate and Atmospheric Science* **2024a**, *7*. https://doi.org/10.1038/s41612-024-00617-1.

Zhang X.; Lei, L; Che H. et al. Aerosol Components Derived from Global AERONET Measurements by GRASP: A New Value-added Aerosol Component Global Dataset and its Application. *Bulletin of the American Meteorological Society* **2024b**, *105* (10), E1822–E1848. https://doi.org/10.1175/BAMS-D-23-0260.1.

Zhang, X.; Gui, K.; Zhao, H. et al. Real-time Mapping of Gapless 24-hour Surface PM10 in China. *National Science Review* **2025**, *12* (2). https://doi.org/10.1093/nsr/nwae446.

WMO SDS-WAS websites and contacts

WMO SDS-WAS:
https://community.wmo.int/en/activity-areas/gaw/science-for-services/sds-was
Email: gaw@wmo.int

Regional Centre for Northern Africa, Middle East and Europe (NAMEE):
http://dust.aemet.es Email: dust@aemet.es

Regional Centre for Asia:
http://www.asdf-bj.net/ Email: xiaoye@cma.gov.cn

Regional Centre for the Americas:
http://sds-was.cimh.edu.bb/ Email: asealy@cimh.edu.bb

Regional Centre for Gulf Cooperation Council (GCC) Countries:
http://dust.ncm.gov.sa/ Email: sdsc@ncm.gov.sa

All authors (in alphabetical order)

Melanie Ades, Saud Alamoudi, Sultan Alduaji, Turki Alharbi, Juan Carlos Antuña-Marrero, Shunsuke Aoki, Sara Attarchi, Victoria Cachorro, Emanuele Emili, Johannes Flemming, Ángel de Frutos, Gerardo García-Castrillo, Carlos Pérez García-Pando, Thomas E. Gill, María Gonçalves, Ke Gui, Qi Jiang, Saviz Sehat Kashani, Takuji Kubota, Li Lei, Alaa Mhaswish, Masataka Muto, Scott Van Pelt, Mehdi Rahnama, Samuel Remy, Toshiyuki Tanaka, Enza Di Tomaso, Tsuyoshi Thomas Sekiyama, Yaqiang Wang, Ernest Werner, Peng Xian

World Meteorological Organization wmo.int

JN 25645